12-1-2017

Development of a Multiphase Photon Monte Carlo Method for Spray Combustion and its Application in High-pressure Conditions

Somesh Roy
Marquette University, somesh.roy@marquette.edu

Jian Cai
University of Wyomming

Michael F. Modest
University of California, Merced

Accepted version. *International Journal of Heat and Mass Transfer*, Vol. 115, Part A (December 2017): 453-466. DOI.

Development of a multiphase photon Monte Carlo method for spray combustion and its application in high-pressure conditions

Somesh P. Roy[1], Jian Cai[2], and Michael F. Modest

University of California, Merced, CA, USA

Abstract

In this work the development of a multiphase photon Monte Carlo (PMC) method with a focus on resolving radiative heat transfer in combustion simulations is presented. The multiphase PMC solver can account for description of participating media in both Lagrangian and Eulerian frameworks. The solver is validated against exact solutions in several one-dimensional configurations. The developed solver is then applied to Diesel spray combustions, where liquid spray droplets are assumed to be cold, nonemitting, large, and isotropically scattering. Several formulations for radiative properties of the Diesel spray are first explored. The PMC solver has then been coupled with the multiphase spray combustion solver in OpenFOAM and the coupled solver is used for simulations of high pressure Diesel spray combustion. It was found that in typical Diesel spray combustion applications, such as in an internal combustion engine, impact of radiation on the evolution of the liquid spray was insignificant. Although the impact of radiation on the spray was minimal, nongray spectral properties and the assumption of semi-transparency for Diesel spray were found to impact the radiative transfer significantly, while impact of scattering was marginal. Spray radiation was also found not to have much effect on global combustion characteristics in high-pressure engine-relevant configurations. However, a small but noticeable effect on minor species distribution relevant to pollutant formation was observed.

Keywords: Monte Carlo radiation solver; multiphase radiation; Diesel spray; high-pressure spray combustion; internal combustion engine

1. Introduction

High-fidelity combustion simulations require accurate modeling of turbulence, chemistry, and radiative heat transfer. Each of these processes is mathematically complex and computationally expensive. These processes closely interact with each other. Hence, to resolve accurate physics of a combustion system each of these three processes should be modeled with comparable fidelity. However, due to the small influence of radiation on small scale laboratory flames and due to the computational complexity of radiation solvers, radiation modeling in combustion simulations is usually less sophisticated than flow or chemistry modeling. Although such simplification may be satisfactory for simple and small geometries at atmospheric pressure, it is generally not appropriate for practical combustion systems.

Combustion processes in many practical systems are heterogeneous; for example, coal furnaces or internal combustion engines (ICEs). It is the presence of the discrete phase that makes multiphase radiation modeling a hurdle in such combustion simulations. Multiphase radiation modeling involves models for both the continuum carrier or gas phase and the discrete dispersed or particulate phase. The optical regime of particulates depends on their size, complex index of refraction, and the irradiating wavelength. Wide variability in these parameters makes accurate radiation modeling in particulate media a daunting task. While a large body of work exists on modeling radiation for dispersed and particulate media [1, 2, 3, 4, 5], not many studies have been done on radiation in the context of multiphase combustion, and even fewer studies focused on multiphase radiation in high-pressure spray combustion.

[1]Corresponding author. Email: somesh.roy@marquette.edu. Current affiliation: Marquette university, Milwaukee, WI, USA.
[2]Current affiliation: University of Wyoming, Laramie, WY, USA.

In spray combustion, the thickness of the reaction zone and droplet diameter are often of the same order, thereby making flame dynamics very sensitive to spray evolution [6]. Evolution of spray, on the other hand, is sensitive to heating of the spray due to convection and radiation. In a single droplet study Godsave [7] estimated that for large benzene droplets, radiation could contribute as much as 20% of the heat of evaporation in the presence of hot surroundings. For a monodisperse spray in an inert atmosphere, Sazhin et al. [8] reported a small but noticeable effect of radiation on Diesel droplet surface temperature and evaporation rate, particularly for larger droplets. In single droplet studies in microgravity [9] and in low-pressure [10], radiation has also been shown to affect droplet evaporation rate under certain conditions. For hydrocarbon fuels Tseng and Viskanta [11] showed that depending on the relative rate of heat transfer due to radiation and convection, evaporation of droplets is affected by radiation in a combustion environment. They also showed that for n-heptane droplets of 100 μm diameter, radiative heating could be as high as 15% of convective heating in presence of 1000 K surroundings.

For an order-of-magnitude analysis of relative heat transfer rates due to convection and radiation, we assumed a motionless droplet with diameter of $d = 20\ \mu$m and uniform temperature of $T = 300$ K in a unit volume of still ambiance of radiatively inert gas at $T_\infty = 800$ K in a closed chamber whose walls are black and hot (same temperature as the surrounding combustion gas). If one assumes the droplet to be large and opaque with an absorption efficiency of $Q_{abs} = 0.95$, and it being uniformly irradiated with radiation from a black surrounding at $T_{comb} = 2000$ K. The approximate convective and radiative heat transfer rates for the droplet, respectively, would be

$$S_{conv} \approx \frac{\mathrm{Nu} \times k}{d} \pi d^2 (T_\infty - T), \tag{1}$$

$$S_{rad} \approx Q_{abs} \pi \frac{d^2}{4} \sigma T_{comb}^4, \tag{2}$$

where Nu is the Nusselt number, σ is the Stefan-Boltzmann constant, and k is the conductivity of the droplet. Assuming a droplet moving with the surrounding gas (*i.e.*, no relative velocity, hence, Nu = 2) and a liquid fuel conductivity of $k \approx 10^{-2}$ Wm^{-1}K^{-1}, one obtains $S_{rad}/S_{conv} \approx 0.4$. This indicates that under some conditions radiative and convective heat transfer could be comparable. Although in practical high pressure spray combustion systems this ratio, S_{rad}/S_{conv}, is expected to be small because of the high rate of convective heat transfer owing to high injection velocity, it is important to confirm the impact of multiphase radiation in such conditions with a rigorous quantitative analysis.

Several studies have been carried out on the effects of radiation in the context of fire and quenching by spray or mist [12, 13, 14, 15, 16, 17, 18, 19, 20]. Some spray combustion studies, such as [21] and [22], had included radiation but only for the gas-phase. Very few studies were in the context of spray combustion that included multiphase radiation. Based on the findings of [11], Watanabe et al. [23] investigated the impact of radiation in spray combustion in a laminar counterflow n-heptane flame using a discrete ordinates method (DOM) for radiation. They found that consideration of the spray in the radiation model does not affect the temperature field substantially, but affects soot production. Building on [23], recently Fujita et al. [24] performed a simulation of a jet flame with n-decane as liquid spray fuel coupled with multiphase radiation calculations using a narrow band model and a DOM solver. There appears to have been very few studies that considered multiphase radiation in the context of practical spray combustion systems, such as ICEs. Very recently, El-Asrag et al. [25] performed a coupled large eddy simulation of a Diesel engine with optically thin multiphase radiation.

The primary goals of this work are to develop an accurate and efficient multiphase radiation solver suitable for combustion simulations, to evaluate accuracy, applicability, and sensitivity of various optical models for radiation formulation of Diesel fuel in spray combustions. To that end, a multiphase photon Monte Carlo (PMC) method is developed for accurate analysis of radiative heat transfer coupled with flow and combustion in the presence of a discrete phase, specifically, liquid fuel spray. This solver is then used to evaluate impact of multiphase radiation in

spray combustion in an engine-relevant condition. Although the solver is developed with high-pressure Diesel spray in mind, it can be used, with minor modifications, for any coupled combustion simulations where a discrete phase is present.

The broader goal of the current work is to advance the understanding of the spray combustion dynamics in engines. Several studies have shown importance of radiation in engine [26, 27, 28, 29, 30]. In most previous studies without radiation, turbulence, chemistry, and spray models are usually "tuned" to match global experimental data such as spray penetration length and ignition delay on a case-by-case basis. Instead of tuning the spray, combustion, or turbulence models, in this work we used standard versions of these models as available in the literature and focused specifically at the quantitative evaluation of the effect of multiphase radiation on spray.

The solver developed in the current work was implemented on the open source OpenFOAM [31], utilizing its built-in spray modeling capabilities. The developed multiphase PMC solver is designed to handle both a Lagrangian and a Eulerian description of the discrete phase. In this article we first discuss the models for radiative property calculations for the discrete phase, followed by a description of the Eulerian-PMC and the Lagrangian-PMC schemes developed and used in the current study. Then we present validation studies and sensitivity studies for the optical models used in modeling spray radiation properties. The multiphase PMC scheme is then used to evaluate the effect of radiation on the evolution of the spray and the impact of including the spray in radiation calculations in configurations relevant to an internal combustion engines. It is emphasized here that the primary motivation of this work is to develop a multiphase radiation model, and not to investigate spray, chemistry, and combustion models, or their interaction directly.

2. Calculation of radiative properties of droplets

Radiative properties of a droplet of radius a, when interacting with a ray of wavelength λ, are governed by three nondimensional parameters: *i*) complex index of refraction, $m = n - ik$; *ii*) size parameter, $x = 2\pi a/\lambda$; and *iii*) clearance-to-wavelength ratio, c/λ. Here we assume independent scattering ($c/\lambda \gg 1$), thereby removing the effect of clearance-to-wavelength ratio from the formulation. Absorption and scattering potential of a droplet is expressed in terms of efficiency factors. Efficiency factors for absorption, scattering, and extinction for a droplet of radius a are given as [32]

$$Q_{abs} = \frac{C_{abs}}{\pi a^2}, \qquad Q_{sca} = \frac{C_{sca}}{\pi a^2}, \qquad Q_{ext} = \frac{C_{ext}}{\pi a^2} = \frac{C_{abs} + C_{sca}}{\pi a^2}, \tag{3}$$

where C_{abs}, C_{sca}, and C_{ext} are absorption, scattering, and extinction cross-sections, respectively.

Calculation of radiative properties of droplet involves *i*) evaluation of spectral variation of complex index of refraction of the liquid fuel and *ii*) formulation for absorption and scattering efficiencies of droplets. In this work we explore several models and formulations for both of these aspects of droplet radiative properties.

2.1. Complex index of refraction of liquid fuel

The choice of liquid spray of the current study is Diesel fuel. Because of the complexity of real fuel, *n*-heptane is often used as a surrogate in both experimental studies and numerical simulations of Diesel combustions. Surrogates are determined by matching various properties such as density, evaporation characteristics, C/H ratio, ignition timing, sooting propensity, etc. with the target fuel. Choice of surrogate fuel usually depends on the focus of the application at hand, for example, the surrogate to study global characteristics of an engine may be different than surrogate used to look specifically at the emission characteristics. Common Diesel surrogates such as *n*-heptane, *n*-decane, *n*-dodecane, and various combinations thereof are primarily based on the chemical and physical properties of Diesel fuel. Although heptane is a reliable chemical surrogate for Diesel fuel, it may not be a very reliable surrogate in terms of spectral

radiative properties. Unfortunately, not a great amount of reliable and standard data exist for spectral properties of real Diesel fuel.

The complex index of refraction ($m = n - ik$) for n-heptane (and n-decane) was studied by Tuntomo [33] for the mid-infrared range (2–10 μm). He found that, while the refractive index (n) showed only small variations, the index of absorption (k) varied wildly by two orders of magnitude in this range. Dombrovsky and coworkers [34, 35, 4] have studied spectral radiative properties of different grades of Diesel, and found these to be indeed different from n-heptane. They also noted that the spectral properties of Diesel fuel vary substantially with the grade and condition (*e.g.*, source, composition, age, etc.) of the fuel. The variation among grades of Diesel is more prominent in the index of absorption than in the refractive index. Although the index of absorption for n-heptane and different grades of Diesel are of the same order, severe differences exist in locations and magnitudes of individual peaks and troughs of the spectral profile [34]. In general it was found that for Diesel fuel,

$$\left.\begin{array}{ll} n & \sim O(1.5) \\ k & \sim O(10^{-4} - 10^{-1}) \end{array}\right\} \text{ for } \lambda \in (2, 10)\ \mu\text{m}. \tag{4}$$

Reliable spectral data for Diesel fuel at $\lambda < 2$ μm or $\lambda > 10$ μm appear unavailable. In this work, a table of n and k was constructed from the data reported by [34] for unboiled Diesel fuel for automobiles. A reconstruction this data is shown in Appendix A. A simple correlation to fit the above data was later proposed by [4]. This correlation is also used in the current work for sensitivity analysis:

$$n(\lambda) = n_0 + 0.02\frac{\lambda - \lambda_m}{(\lambda - \lambda_m)^2 - 0.001}, \tag{5a}$$

$$k(\lambda) = 10^{\gamma}, \tag{5b}$$

where the wavelength, λ, is measured in μm. The correlation constants (n_0, λ_m, and γ) used in the current work are given in Appendix B.

2.2. Optical models for droplets

The range of diameters for spray droplets lies between a few to a few hundred micrometers; whereas the irradiating wavelength in typical combustion application is mainly around 2–5 μm. Therefore, in most cases spray droplets can be considered as large droplets (*i.e.*, $x \gg 1$) and can be assumed to follow geometric optics. For heat transfer applications, diffraction from large droplets can be treated as transmission, and hence can be neglected [32]. It can be shown that for large droplets without diffraction the extinction efficiency for wavelength λ is unity,

$$Q_{ext,\lambda} = 1. \tag{6}$$

2.2.1. Opaque droplets

If we also assume the droplets to be largely opaque so that any ray refracted into the droplet will be completely absorbed (*i.e.*, $kx > 1$), the scattering and absorption efficiencies, respectively, reduce to hemispherical reflectance and absorptance. On a spectral basis,

$$Q_{sca,\lambda} = \rho_\lambda, \qquad Q_{abs,\lambda} = \epsilon_\lambda, \tag{7}$$

where ρ_λ is the hemispherical reflectance and ϵ_λ is hemispherical absorptance or hemispherical emittance averaged over all incoming/outgoing directions for wavelength λ. For brevity, we omit the subscript λ in the rest of the document.

Calculation of the hemispherical reflectance and absorptance depends on the complex index of refraction and not on the size of the droplet. Several idealized approximations have been reported in [32]. Here we use two approximations for hemispherical reflectance.

The first and simplest approximation for hemispherical reflectance is to use a formulation for normal incidence on a large sphere. Using Fresnel's relations, the reflectance for unpolarized rays due to normal incidence can be written as

$$\rho = \frac{(n-1)^2 + k^2}{(n+1)^2 + k^2}. \tag{8}$$

A more involved formulation for hemispherical emittance for different ranges of n and k was first proposed by Dunkel [36, 32] as a combination of emittance of parallel and perpendicular polarizations. For fuel sprays, $k^2 \ll n^2$, and the hemispherical emittance can be approximated as per Dunkel's relation for nonconductors [32]

$$\epsilon_{\parallel} = \frac{4(2n+1)}{3(n+1)^2}, \tag{9a}$$

$$\epsilon_{\perp} = \frac{4n^3(n^2+2n-1)}{(n^2+1)(n^4-1)} + \frac{2n^2(n^2-1)^2}{(n^2+1)^3}\ln\left(\frac{n+1}{n-1}\right) - \frac{16n^4(n^4+1)\ln n}{(n^2+1)(n^4-1)^2}, \tag{9b}$$

$$\epsilon = \frac{1}{2}\left(\epsilon_{\parallel} + \epsilon_{\perp}\right). \tag{9c}$$

2.2.2. Semi-transparent droplets

Calculations of extinction efficiency via Eqns. (8) – (9) are based on geometric optics and only valid for large and opaque droplets. Because of the small index of absorption of Diesel fuel, the assumption of opaque droplet ($kx > 1$) is not always appropriate. Particularly in combustion environment, small droplets become semi-transparent [11]. An alternate size-based correlation for absorption efficiency for semi-transparent droplets was proposed by [37]. This correlation is applicable for the cases when $k \ll 1$ and $x \gg 1$, and was tested against Mie calculations. The absorption efficiency according to this correlation is

$$Q_{abs} = \frac{4n}{(n+1)^2}\left(1 - \exp(-4kx)\right). \tag{10}$$

In this study we used the above three optical formulations: the normal incidence approximation [Eqn. (8)], Dunkel's relation [Eqn. (9)], and the semi-transparent correlation [Eqn. (10)] to perform a sensitivity study. In all cases, the dispersed medium is assumed to be isotropically scattering only.

2.3. Spray representation

In a typical spray combustion simulation, droplets of various sizes will be distributed over the entire computational volume. For a distribution of droplets in a finite computational volume (V), the total number of droplets per unit volume is given by

$$N_T = \int_0^{\infty} \nu(a)da, \tag{11}$$

where $\nu(a)$ is the droplet number density function. For a discrete-sized droplet distribution, the integrations over the number density can be transformed to summations with delta functions as

$$N_T = \frac{1}{V} \sum_{i \in \mathcal{N}^d} N_i \delta(a - a_i), \tag{12}$$

$$\kappa = \frac{\pi}{V} \sum_{i \in \mathcal{N}^d} N_i Q_{abs,i} a_i^2, \tag{13}$$

$$\sigma_s = \frac{\pi}{V} \sum_{i \in \mathcal{N}^d} N_i Q_{sca,i} a_i^2, \tag{14}$$

where N_i is the number of droplets of radius a_i and $\mathcal{N}^d$ represents the discrete droplet population set.

Since the current implementation of our photon Monte Carlo scheme for sprays is based on the open source OpenFOAM code suite, it is worth noting here that instead of modeling each droplet individually, in OpenFOAM, sprays are numerically represented as a set of 'parcels.' Each parcel contains several droplets of identical properties. The number of droplets in a parcel is derived from the liquid-phase mass balance and hence can be a noninteger. This description of spray inherently assumes that inside a parcel, all droplets are spatially collocated on one single coordinate as indicated in the parcel and they are subjected to the same external influences such as drag force, heat transfer, etc.

3. Photon Monte Carlo method

In this section the method of multiphase photon Monte Carlo (PMC) solver is discussed. First the basics of the method is presented, followed by two different approaches (Eulerian and Lagrangian) for ray tracing and interaction with participating media and the scheme for energy accounting across different phases. The choice of Eulerian or Lagrangian PMC can be made depending on how the participating media is represented in the main combustion solver.

3.1. Photon rays and participating media

In the photon Monte Carlo (PMC) method radiative transfer in participating media is solved by emitting and tracking a finite set of photon bundles or rays in the domain. The total energy contained in the photon bundles is the same as the total emission from the computational domain. In typical spray combustion the temperature of droplets is much lower than that of combustion gases. Total energy emitted from the spray phase is, thus, very small compared to that emitted from the gas-phase. Therefore, droplets are assumed to be nonemitting and only take part in absorption and scattering. Emission from the k^{th} finite volume cell is characterized by

$$\begin{aligned} \mathcal{E}_{emi,k} &= 4 P_k V_k \kappa_{P_p,k} \sigma T_k^4, \\ &= 4 P_k V_k \sigma T_k^4 \sum_{i \in \mathcal{N}_{sp}} \kappa_{P_p,i,k} x_{i,k}, \end{aligned} \tag{15}$$

where P_k, V_k, and T_k are, respectively, the total pressure, the total volume, and the temperature of the emitting medium in cell k, $x_{i,k}$ and $\kappa_{P_p,i,k}$ are mole fraction and pressure-based Planck-mean absorption coefficient for species i in the cell, and $\mathcal{N}_{sp}$ is the set of radiatively participating species. This energy is emitted via a finite number of rays in a way that the total energy emitting from a cell is conserved; *i.e.*, if there are N_k rays emitted from a finite-volume cell k, each ray carries an amount of energy, $E_j = \mathcal{E}_{emi,k}/N_k, \forall j \in \mathcal{N}_k^{r,em}$, where $\mathcal{N}_k^{r,em}$ is the set of rays emitted from cell k. Each ray, which can have one or more wavenumbers associated with it, is tracked until it exits the domain or its energy is

depleted due to interaction with participating media including the droplets. The selection algorithms of emission point, propagation direction, and wavenumbers are based on random number relations and have been reported in [32, 38, 39].

Photon rays can be modeled as line rays or cone rays [38]. The line ray representation is the simplest representation for photon bundles, and involves tracing of a straight line through the computational domain. The cone ray topology, albeit more physical, involves tracing a propagating cone in the computational domain. Both these topologies are used in the current study under appropriate conditions as described later.

To represent the carrier gas phase two approaches have been used: a conventional continuous Eulerian description, and a discrete Lagrangian description. In the discrete Lagrangian representation, a set of stochastic probability density function (PDF) particles on a Eulerian mesh are used to model the gas phase. This approach is the same as the one used in the stochastic transported probability density function (tPDF) method implemented on a hybrid Lagrangian-particle Eulerian-mesh (LPEM) framework [40]. In the current work, a Eulerian-Eulerian PMC (Sec. 3.2) is used in cases where the gas phase is treated as Eulerian and a Lagrangian-Lagrangian PMC (Sec. 3.3) is used when the gas phase is represented using PDF particles.

In the reminder of this article, subscripts i, j, and k are used to represent droplets or parcels, rays, and computational cell, respectively. The sub- and superscripts g and d are, respectively, reserved for gas phase and spray (droplet) phase terms.

3.2. Eulerian-Eulerian PMC

In the Eulerian-Eulerian PMC coupling, radiative properties of the Lagrangian spray parcels are converted to an equivalent Eulerian phase for PMC calculations. Since the Lagrangian identity is lost for ray tracing purpose, only the line ray topology is used in the PMC. In this case, the droplet properties are "distributed" over the entire computational cell. Therefore each ray, in essence, interacts with all droplets present in the cell. The PMC in this framework is referred as Eulerian-Eulerian PMC or simply Eulerian PMC.

Radiative properties of a discrete distribution of spray droplets can be obtained following Eqns. (13) – (14). Since a parcel, i, consists of $N_{p,i}$ identical droplets of radius a_i and absorption efficiency $Q_{abs,i}$, the bulk absorption coefficient due to the parcel in the finite volume cell of volume V can be written as [41]

$$\kappa_{d_i} = \frac{\pi}{V} N_{p,i} a_i^2 Q_{abs,i}. \tag{16}$$

If $\mathcal{N}_k^d$ is the set of parcels present in cell k, then the bulk Eulerian absorption coefficient due to spray parcels is

$$\kappa_{d,k} = \sum_{i \in \mathcal{N}_k^d} \kappa_{d_i}. \tag{17}$$

Therefore, the total optical thickness passed through by ray j in cell k is

$$\tau_{kj} = l_{kj} \left(\kappa_{g,k} + \kappa_{d,k} \right) = \tau_{kj}^g + \tau_{kj}^d, \tag{18}$$

where l_{kj} is the length of travel of ray j through cell k, $\kappa_{g,k}$ is the gas-phase absorption coefficient, and τ_{kj}^g and τ_{kj}^d are, respectively, absorption optical thickness contributions from gas and spray phases.

The above formulation is for absorption only. A similar formulation can be obtained for scattering. Since gases do not scatter appreciably, the optical thickness for scattering can be given as

$$\tau_{sca,kj} = l_{kj} \sigma_{s,d,k} = \tau_{sca,kj}^d, \tag{19}$$

where $\sigma_{s,d}$ is the scattering coefficient for spray droplets.

3.3. Lagrangian-Lagrangian PMC

As mentioned earlier, this approach is implemented with the tPDF method [40], where the carrier gas phase is treated in a Lagrangian manner using stochastic PDF particles. In this approach, each spray parcel retains its Lagrangian identity, and hence a finite volume and a specific location. Therefore, the interaction between a ray and a droplet/parcel takes place based on the origin and direction of the ray and location of the droplet/parcel, irrespective of the finite-volume cell in which the droplet/parcel is located.

Since the volume of a parcel is very small compared to the volume of a computational finite-volume cell, they may be treated as point masses. Hence, the cone-ray topology along with the cone-point particle mass (cone-PPM) scheme [38] is used for both ray–gas and ray–spray interaction. In the cone-ray model, photon rays are assumed to occupy a small solid angle and propagate axisymmetrically along a cone. Intensity of the ray at any location $\mathbf{x}$ is given by

$$I(s, r) = I_0(s) W_{2D}\left(\frac{r}{R_c(s)}\right), \tag{20}$$

where $s = (\mathbf{x} - \mathbf{x_0}) \cdot \hat{\mathbf{s}}$ is the distance from the ray origin $\mathbf{x_0}$, $\hat{\mathbf{s}}$ is direction of the ray, r is the radial distance from the axis of the ray, I_0 is the intensity at the axis, $R_c(s)$ is the radius of influence of the ray at distance s from its origin. W_{2D} is a normalized two-dimensional weight function that describes the radial energy distribution inside the ray such that $\int_0^1 W_{2D}(\varrho) 2\varrho \, d\varrho = 1$ [38]. Here we used the same Gaussian-like function used in [38].

Following the development of [38] and using the discrete distribution of the Lagrangian spray, the optical thickness of point masses inside the cone of influence of the ray j is evaluated as

$$\tau_j = \sum_{i \in \mathcal{N}_j} \kappa_i \frac{W_{2D}(r_i/R_{c,i})}{\pi R_{c,i}^2} V_i = \sum_{i \in \mathcal{N}_j} \tau_{ij}, \tag{21}$$

where $\mathcal{N}_j$ is the set of Lagrangian parcels inside the ray's cone of influence, κ_i, r_i, V_i, and τ_{ij}, respectively, are the absorption coefficient, the radial distance from the cone axis, the volume, and the optical thickness contribution of the parcel i and $R_{c,i}$ is the cone radius at location of parcel i. In terms of spray properties, the optical thickness contribution of parcel i to the ray j can be expressed as

$$\tau_{ij}^d = N_{p,i} a_i^2 Q_{abs,i} \frac{W_i}{R_{c,i}^2}, \tag{22}$$

where $N_{p,i}$ is number of droplets in the parcel, a_i and $Q_{abs,i}$ are, respectively, the radius and absorption efficiency of droplets in the parcel i, and $W_i = W_{2D}\,(r_i/R_{c,i})$ is the point weight of the parcel.

Following Modest et. al. [32, 38], the contribution of local gases to the optical thickness for a ray is represented by τ^g. This simply adds to the optical thickness that the ray encounters traversing spray parcels. Therefore, the total optical thickness that the ray j passes through is

$$\tau_j = \sum_{l \in \mathcal{N}_j^g} \tau_{lj}^g + \sum_{i \in \mathcal{N}_j^d} \tau_{ij}^d, \tag{23}$$

where $\mathcal{N}_j^g$ is the set of stochastic PDF particles and $\mathcal{N}_j^d$ is the set of spray parcels inside the ray's cone of influence. Evaluation of τ_{lj}^g has been described in detail by [38].

The above formulation is for optical thickness due to absorption only. Neglecting scattering by gases, optical

thickness due to scattering can be evaluated in a similar way:

$$\tau_{sca,j} = \sum_{i \in \mathcal{N}_j^d} \tau_{sca,ij}^d = \sum_{i \in \mathcal{N}_j^d} N_{p,i} a_i^2 Q_{sca,i} \frac{W_i}{R_c^2}. \tag{24}$$

Rays are traced from cell to cell. Inside a computational cell, instead of interacting with each parcel/PDF particle individually, first all interacting parcels and PDF particles are searched and collected based on their optical thickness contribution and then energy is dumped on them according to the energy accounting scheme discussed in the next section.

3.4. Energy accounting across phases

A key assumption made in the development of the PMC for spray combustion is the fact that spray droplets are much cooler than surrounding combustion products. Hence emission from spray droplets is negligible compared to that from combustion gases. Therefore, the spray is assumed to be nonemitting, but absorbing and isotropically scattering.

A photon ray gets attenuated by both absorption and scattering. As discussed in [32] an energy partitioning scheme is used to account for absorption of a photon ray inside the medium, while, a ballistic scheme is used to account for scattering. In its course of travel, when the optical thickness due to scattering exceeds a predefined maximum value for a ray, the ray will be scattered, *i.e.*, change its direction without any change in intensity or wavenumber. The predefined maximum value of scattering optical thickness is obtained as

$$\tau_{sca,max} = \ln \frac{1}{R_\sigma}, \tag{25}$$

where R_σ is a random number. Assuming isotropic scattering, the new direction can be determined by random numbers similar to the way the original emission direction was decided. Tracking of the ray then continues the until ray hits a boundary or is completely absorbed.

According to the energy partitioning scheme for absorption, if ray j passes through an absorption optical thickness of τ_{kj} in computational cell k, the energy dumped by the ray on gas and spray phases of cell k is given by

$$\Delta E_{kj} = E_{kj}^0 (1 - e^{-\tau_{kj}}), \tag{26}$$

where E_{kj}^0 is the energy with which ray j entered cell k. Following [42], this energy is distributed across the gas and spray phases as

$$\Delta E_{kj}^g = \frac{\tau_{kj}^g}{\tau_{kj}} \Delta E_{kj}, \tag{27}$$

$$\Delta E_{kj}^d = \frac{\tau_{kj}^d}{\tau_{kj}} \Delta E_{kj}, \tag{28}$$

where ΔE_{kj}^g is the amount of energy absorbed by the gas phase and ΔE_{kj}^d is the amount of energy absorbed by spray parcels. Energy gained by parcel i due to its interaction with ray j in cell k can then be calculated as being proportional to droplet cross-section, or

$$\Delta E_{i,kj}^d = \frac{N_{p,i} a_i^2}{\sum_{l \in \mathcal{N}_k^d} N_{p,l} a_l^2} \Delta E_{kj}^d, \qquad \forall i \in \mathcal{N}_{kj}^d, \tag{29}$$

where $\mathcal{N}^d_{kj}$ is the set of droplets that the ray j passes through in cell k. Since in the Eulerian PMC every ray interacts with every parcel, $\mathcal{N}^d_{kj}$ and $\mathcal{N}^d_k$ are the same.

For combustion applications the most important quantity is the radiative source term, which can be obtained as

$$S_{rad,k} = -\nabla \cdot \mathbf{q} = \frac{1}{V_k}\left(-\mathcal{E}_{emi,k} + \sum_{j\in\mathcal{N}^r_k} \Delta E_{kj}\right), \tag{30}$$

where $\mathbf{q}$ denotes the radiative heat flux and $\mathcal{N}^r_k$ is the set of rays that passes through (including the ones originated from) computational cell k. Since the spray does not emit, radiative source terms for individual phases are obtained as

$$S^g_{rad,k} = \frac{1}{V_k}\left(-\mathcal{E}_{emi,k} + \sum_{j\in\mathcal{N}^r_k} \Delta E^g_{kj}\right) \tag{31}$$

$$S^d_{rad,i,k} = \sum_{j\in\mathcal{N}^r_k} \Delta E^d_{i,kj} \qquad \forall i \in \mathcal{N}^d_k, \tag{32}$$

where $S^g_{rad,k}$ (W/m^3) is the Eulerian source term for gas phase in cell k and $S^d_{rad,i,k}$ (W) is the Lagrangian source term for parcel i in cell k. Note the difference in units for the Lagrangian and Eulerian phases. The source term for an individual droplet in parcel i then can be obtained as $S^d_{rad,i,k}/N_{p,i}$. Further details about energy accounting in stochastic PDF particles representing the gas phase in the Lagrangian-Lagrangian PMC can be found in [38].

4. Results and discussion

In this section we first present validation of the PMC implementation, followed by a parametric study of radiative property models for spray droplets. Results from a series of coupled simulations for a constant-volume combustion chamber is presented next. Finally, we try to appraise the importance of consideration of spray in radiation calculations (as opposed to single-phase, gas-only) in configurations typical for Diesel engines. Results from both the Eulerian-Eulerian and Lagrangian-Lagrangian PMC are shown, compared, and validated in the first subsection. But for the rest of the work, we only used Eulerian PMC owing to the high computational cost of Lagrangian PMC.

The modeling assumptions used in spray radiation are: droplets are large ($x \gg 1$); they are nonemitting; dependent scattering is neglected; and scattering, when considered, is assumed to be isotropic. In the parametric study (Sec. 4.2), droplets are considered as either opaque or semitransparent, depending on the optical model used and the radiative property of Diesel fuel is assumed to be either a spectrally-invariant constant index of refraction or a spectrally dependent function represented by either a correlation [Eqn. (5)] or a line-by-line table [34].

4.1. Validation in a one-dimensional slab

The PMC scheme is validated against exact solutions, which can be obtained only for simple configurations, such as a one-dimensional slab. The one-dimensional slab configuration used for validation is bounded by two black walls 0.1 m apart. Spray parcels are distributed in the finite volume cells in a way that a desired spatial distribution of bulk Eulerian spray absorption coefficient, κ_d, can be obtained. Parcels are made of identical droplets of 5 μm diameter. The number of droplets inside parcels is modified to obtain the desired κ_d distribution in each case. In all tests the droplet radiative properties are assumed to be gray with a complex index of refraction of $m = 1.5 - 2\times10^{-3}i$. This value, although somewhat arbitrary, is in the range of values typical of n-heptane droplets [37]. Droplet absorption efficiencies are calculated using the normal incidence formulation [Eqn. (8)].

Here we only present two validation results for the sake of brevity. The first case considered is without any gas phase, *i.e.*, the slab contained only spray droplets. The bounding top and bottom walls are at a temperature of

T_w = 2000 K. The medium is assumed to be kept isothermal by convective cooling. Since droplets are considered cold and nonemitting, emission comes only from the bounding walls. In this case only one participating phase is present, hence the entire absorption corresponds to absorption by droplets. The number of droplets in a parcel is chosen in this case such that the bulk Eulerian droplet absorption coefficient is $\kappa_d = 10\ \mathrm{m}^{-1}$. Figure 1 shows the comparison of the divergence of heat flux calculated from the Eulerian PMC and from the exact solution. The PMC results match very well with the exact solution.

The second validation case compares both the Eulerian and the Lagrangian PMC with the exact solution. Figure 2 presents a validation result for the one dimensional case with cold black walls and a uniform gas temperature of 1000 K. The participating gases and spray parcels are distributed appropriately to achieve a distribution of bulk absorption coefficient for both phases as shown in the figure. Results from the Eulerian and the Lagrangian PMC match very closely with the exact solution for each phase. Since the standard deviation of the PMC results are very small compared to the mean value, error bars are omitted in this and all subsequent figures. Computational costs for the PMC simulations are dominated by the cost of ray tracing. Since cone-PPM tracing involves a more expensive search than line ray tracing, the Lagrangian PMC is generally expected to be more costly than the Eulerian PMC. It was found that in this configuration, for the same number of rays, the Lagrangian PMC was approximately 12 times more costly than the Eulerian version. Results presented in the rest of this work are obtained from the Eulerian PMC.

4.2. Sensitivity to droplet radiative property models

The effects of different complex indices of refraction and absorption efficiency formulations for droplets are explored in a snapshot from a constant volume combustion chamber simulation (the `aachenBomb` tutorial in OpenFOAM-2.2.x [31]). The configuration consists of a 0.02 m $\times$ 0.1 m $\times$ 0.02 m rectangular cuboid discretized into 168,100 cells. The cube is filled with air at 800 K and 50 bar at the start of the spray injection. The initial size distribution of the injected spray follows a Rosin-Rammler distribution, and is injected at the center of the face at y = 0.1 m. Heptane is treated as a chemical and physical surrogate for Diesel fuel in the simulation. This configuration was simulated with a global one-step chemistry and without radiation until there was significant amount of hot combustion products present in the domain along with cold spray droplets to obtain a snapshot of the configuration. A parametric study on spectral variation of complex index of refraction and optical formulations of the spray droplets was carried out on the snapshot presented in Fig. 3. Sizes of the parcels in the snapshot are scaled according to the diameter of the droplets in the parcels, whereas the colors indicate the number of droplets in each parcel (`nParticle`). The snapshot shows that away from the nozzle spray droplets break up into smaller droplets leading to smaller diameters of droplets and larger `nParticle` in each parcel. Gas phase spectral properties are evaluated using a line-by-line (LBL) database of CO_2 and H_2O obtained from the HITEMP spectroscopic database [43], while the walls of the cube are assumed to be cold and black at 300 K for the parametric study.

4.2.1. Variation in complex index of refraction

As discussed before, the complex index of refraction of Diesel fuel varies considerably with the grade of fuel [4]. The variation is more pronounced in the absorptive index (k) than in the refractive index (n).

In the current work, the spectral variation of the complex index of refraction is modeled in two ways: *i*) using a spectral table (a line-by-line table obtained by digitizing the data presented in [34], which is reconstructed in Appendix A), and *ii*) using the spectral correlation given by Eqn. (5). It is important to note here that reliable spectral data for Diesel fuel are only available for $\lambda \in [2, 10]\ \mu$m, whereas the LBL database for participating gases covers absorption coefficients for the entire relevant range of 0.5 to 50 μm. In the range $\lambda \in [2, 10]\ \mu$m, except for two absorption peaks, around 3.5 μm and 6.5 μm, the absorptive index (k) for Diesel fuel is very small ($\sim O(10^{-3})$).

Assuming absence of any other absorption peak beyond this range, we extended the spectral data beyond the available limits as $n|_{\lambda<2\mu\text{m}} = n|_{\lambda=2\mu\text{m}}$, $n|_{\lambda>10\mu\text{m}} = n|_{\lambda=10\mu\text{m}}$, and $k|_{\lambda<2\mu\text{m}} = k|_{\lambda>10\mu\text{m}} = 0$. The spectral correlation is only valid for $\lambda \in [2, 6]$ μm. For parity with the spectral table, the correlation has been extended as $n|_{\lambda<2\mu\text{m}} = n(\lambda)|_{\lambda=2\mu\text{m}}$, $n|_{\lambda>6\mu\text{m}} = n(\lambda)|_{\lambda=6\mu\text{m}}$, $k|_{6\mu\text{m}<\lambda\leq10\mu\text{m}} = k(\lambda)|_{\lambda=6\mu\text{m}}$, and $k|_{\lambda<2\mu\text{m}} = k|_{\lambda>10\mu\text{m}} = 0$, where $n(\lambda)$ and $k(\lambda)$ are functional forms from Eqn. (5). A third model used in this study assumes no spectral variation of spray properties. This "gray" spray is represented by a constant complex index of refraction, which is determined – somewhat arbitrarily – by visual inspection of the spectral complex index of refraction; the value used here is $m = 1.46 - 0.001i$ ($\forall\lambda \in (0.5, 50)$ μm). Unless otherwise mentioned, in all subsequent cases gray spray refer to this complex index of refraction.

The three spectral models are used with the semi-transparent correlation for absorption efficiency [Eqn. (10)] on the same snapshot. Scattering was neglected in this test. Figure 4 presents profiles of bulk Eulerian-equivalent absorption by the spray phase from the three spectral models along the center of the cuboid. Differences in spray absorption obtained from different spray models are large. The spectral correlation results in minimum absorption because it only captures one absorption peak (~ 3.5 μm) of the fuel. The tabulated data produce maximum absorption, whereas the gray assumption leads to absorption between the other two cases. Again, it is emphasized that the gray complex index of refraction was chosen somewhat arbitrarily, and since the gray assumption implies that the spray absorbs equally at all emitted wavelengths (as opposed to being non-absorptive for $\lambda < 2$ μm and $\lambda > 10$ μm), changing the gray complex index of refraction may change this trend. The variation in the index of refraction (n) is fairly small across the three models, and effects of variations of the index of absorption (k) are attenuated by the exponential factor in the formulation of absorption efficiency [Eqn. (10)]. On the other hand, since Dunkel's relation only involves n, relative differences between spectral models using Dunkel's relation were found to be considerably smaller than those with the semi-transparent correlation. In terms of computational cost, all three models were found to be comparable. Effective computational cost for gray calculations is the least whereas that using the table or correlation are 5% greater.

4.2.2. Variation in optical formulations

Before determining the effects of optical models on spray radiation, we explored the range of values of key parameters in the spray. Figure 5 presents values of absorption efficiencies obtained from different optical formulations while interacting with a ray at 3 μm. The index of refraction for the droplet is assumed to be $n = 1.46$. Since the absorption efficiency from the semi-transparent correlation depends on size parameter (x), we have used five different droplet radii. Over the relevant range of absorption indices (k) for Diesel fuel, the normal incidence approximation yields the highest absorption efficiency, followed by Dunkel's relation. For the most part, $k \in [0.001, 0.01]$ for Diesel fuel, and droplet diameters are in the range of few to few tens of microns. The values of absorption efficiencies from the semi-transparent correlation for this range, shaded in Fig. 5, are significantly smaller than those obtained from the normal incidence approximation or from Dunkel's relation. This indicates that for the current conditions, droplets are semi-transparent, as previously indicated by [11]. Another point of note is that in the relevant range, the absorption efficiency obtained from Dunkel's relation is approximately 95% of that obtained from the normal incidence approximation.

We also explored the probability density function (PDF) of the size parameter (x) and the droplet diameter for the spray in the snapshot. It was found that most droplets have diameters of less than 50 μm. While no common trend was found between the PDFs, and the spatial distribution of PDFs would vary greatly with spray model and injection parameters, size parameters were found to be less than 100 in most cases. Therefore, the approximation of opaque droplets may be less accurate than the semi-transparent correlation. Another point to note here is that in the limit of $k \to 0$, the semi-transparent correlation approaches the normal incidence approximation. Using the large droplet assumption, a modification of the semi-transparent correlation to asymptotically reach the value obtained by Dunkel's

relation at $k \to 0$ may be more accurate. However, in this study, we did not make any such modifications, and used the original formulation.

From the above discussion, we expect that absorption by the spray will be least when the semi-transparent correlation is used to evaluate the absorption efficiency, and will be maximum when the normal incidence approximation is used. This is evident from Fig. 6(a), which presents the amount of absorption obtained from different optical formulations using the spectral table. Moreover, since the difference between the normal incidence approximation and Dunkel's relation is only $\sim 5\%$, absorption by the spray using these two approximations lie very close to each other. In this figure we also explore the effect of scattering. Since the absorption efficiency from the semi-transparent correlation is much smaller than that obtained from other formulations, impact of scattering is expected to be most with this correlation. But even in this case, the effect of scattering is insignificant, *i.e.*, the difference in absorption by the spray with and without scattering is very small.

Figure 6(b) shows the impact of the spray radiation model on local radiative source terms for the gas phase. The gas phase radiative source from single phase (gas-only) radiation (*i.e.*, ignoring the spray in radiation calculations) is also presented in this figure for comparison. Since both the normal incidence approximation and Dunkel's relation yield substantially more absorption by the spray, they also lead to lower absorption by the gas phase. Use of the more realistic semi-transparent correlation yields a gas phase radiative source very close to single phase calculations. Again, inclusion of scattering does not impact the gas phase radiative source significantly. These results tend to indicate that inclusion of a realistic spray in radiation calculations may have small, if at all any, direct impact on the gas phase radiation calculations under these conditions. Impact of multiphase radiation may enter through coupled calculations, where the evolution of the spray may be influenced by the spray radiation model. This is studied in the next section. Finally, it was found that computational costs of different optical models with and without scattering are essentially the same.

4.3. Coupled simulation

As the parametric study suggests, absorption by sprays is sensitive to the spectral and optical models used for spray radiation. The differences using various combinations of models can lead to almost an order of magnitude difference in radiative source terms. This could potentially impact evaporation of spray in combustion environments and hence change the combustion dynamics. In this section we explore the effect of including multiphase spray radiation in coupled combustion simulations. The combination of gray spectral properties with constant index of refraction and the normal incidence approximation gives the most simplified absorption model for the spray, whereas tabulated spray properties with the semi-transparent correlation is the most "physical" model for spray radiation. We restrict our study to these two combinations of spray radiation models. To explore the effects of multiphase radiation, we first investigate a constant-volume combustion system (a.k.a. combustion bomb), and then an engine-relevant configuration.

All these simulations were performed in an unsteady Reynolds' average simulation (RAS) framework using standard compressible $k-\varepsilon$ turbulence model with model parameters $C_{1\epsilon} = 1.44$, $C_{2\epsilon} = 1.92$, $C_3 = -0.33$, $C_\mu = 0.09$, $\sigma_k = 1$, $\sigma_\epsilon = 1.3$, and $Pr_t = 1$ and standard wall functions [44, 31]. A summary of submodels and assumptions used in these simulations is given in Table 1. Further details of these submodels are discussed in respective sections.

4.3.1. A high-pressure combustion bomb

The combustion bomb configuration is the same as the one described in Section 4.2. A spray of 6×10^{-6} kg of *n*-heptane is injected over 1.25 ms at the center of the face at $y = 0.1$ m using a cone-nozzle injector. The nozzle diameter is 190 μm and spray cone angle is 10°. The inlet velocity of droplets is calculated using the nozzle discharge coefficient of 0.9 and injection pressure and temperature [31]. The droplet diameter is determined following a Rosin-Rammler distribution. The minimum and maximum diameters for the distribution is 1 μm and 150 μm, and the

spreading parameter is taken as 3 [31]. No primary atomization model was used and the Rosin-Rammler distribution for droplets is assumed to accommodate the effect of atomization as suggested by [45, 46]. The secondary breakup of spray is modeled using the Reitz-Diwakar breakup model [47, 48, 49]. To minimize model uncertainty, dispersion, stochastic collision, and surface film effects are neglected in this case. Spray parcels are assumed to rebound upon hitting walls. The temperature of the incoming spray droplets is kept at 320 K. Initial pressure and temperature of the combustion chamber are, respectively, 50 bar and 800 K. Chemistry is simulated using a simple global reaction with five species (C_7H_{16}, O_2, CO_2, H_2O, and N_2). It is noted here that the goal of this simulation is to look at the effect of spray radiation and not to investigate accuracy of spray or combustion submodels.

Four coupled simulations are run for the combustion bomb: *a*) without radiation, *b*) with single-phase (gas only) radiation, *c*) with a realistic multiphase radiation model, *i.e.*, using the tabulated spray properties with the semi-transparent correlation, and *d*) with a simple multiphase radiation model, *i.e.*, using gray spray properties with the normal incidence approximation. Case (*a*) is the baseline case. Differences between cases (*b*) and (*c*) illuminate the effects of spray radiation, and differences between cases (*c*) and (*d*) represent the impact of gray and opaque assumptions for the spray on radiation. As indicated earlier, gas phase spectral properties are evaluated using a LBL database for CO_2 and H_2O.

Figure 7 shows the evolution of the liquid spray for all cases. The evaporated liquid mass gives an indication of spray evaporation rate, whereas the liquid penetration length (defined by the distance to which 95% by mass of liquid penetrates from the injection point) represents the spread of the spray. The impact of different radiation models can barely be seen in the profiles shown in this figure. It is clear that radiation does not affect either the global evaporation rate or the liquid penetration length. This is an indication that radiation does not directly influence global spray evolution characteristics. To explore this further, we looked into individual source terms for the energy equation of spray droplets using the spray snapshot shown in Fig. 3. Since the spray is injected into a hot medium, droplets gain energy due to convective and radiative heat transfer, and lose energy due to phase change. It was found that the magnitude of the convective heat transfer rate for each spray parcel at a snapshot of the simulation (*cf.* Fig. 3) was several orders of magnitude larger than the radiative heat transfer rate. It is important here to note that convective heat transfer is modeled using the Ranz-Marshal correlation [50]. Due to the high injection velocity, the Nusselt numbers for droplets are quite large in this case. This, along with small droplet diameter, leads to much larger energy transfer due to convection than radiation. It was also noted, that because of closeness to a strong emission source (hot CO_2 and H_2O), the radiative heat transfer rate is slightly higher for droplets away from the nozzle.

In an effort to find out if there exists any possible scenario in the combustion bomb configuration where multiphase radiation will affect spray evolution, a hypothetical case was constructed. Spray spectral properties are modeled using the tabulated data, and droplet absorptance is calculated using the normal incidence approximation, leading to maximum possible absorption. The walls are assumed to be hot (1000 K) and black. The gas inside the combustion chamber is assumed to be at 330 K, so that the temperature difference potential for convective heat transfer is very small, but not absent. Finally, we neglect phase change, so that the only energy transfer is due to convection and radiation. Relative magnitudes of convective and radiative heat transfer in this hypothetical scenario are presented in Fig. 8. Even in this unphysical extreme scenario, convective heat transfer is larger than radiative heat transfer. Radiative and convective heat transfer are of the same order for only a few droplets. It was found that droplets for which radiative and convective heat transfer rates are comparable are the droplets closer to the nozzle. This is because of the facts that the primary emission source is the wall and droplet diameters are larger near the nozzle. Since convective heating of droplets is orders of magnitude larger than radiative heating even in the unphysical extreme scenario, it is expected that in high pressure cases, such as this, radiative heating for sprays will likely be negligible compared to convective heating.

4.3.2. An engine-relevant conditions

The constant volume combustion configuration showed that radiative heat transfer to droplets is negligible compared to convective heat transfer. We now explore whether similar trend holds true in typical engine-relevant conditions. To this end, we constructed a hypothetical Diesel engine revolving at 1200 rpm with eight azimuthally equispaced injectors with a compression ratio of 15, a displacement volume of 3.21×10^{-3} m^3, and bore of 0.14 m. The dimension and characteristics of the engine, although chosen somewhat arbitrarily, represent typical Diesel engines [51, 52]. Initial mean pressure and temperature at bottom dead center (BDC) is assumed to be 1.5 bar and 320 K. The cylinder head and piston are assumed to be kept at a constant temperature of 800 K, whereas the cylinder wall is kept at 600 K. Since one of our objective is to see if radiation affects spray evolution under extreme conditions, the temperature of walls are assumed to be much higher than that is expected in real engines ($\sim$ 500 K) to exaggerate any effect of wall radiation on spray evolution before and during initial phases of ignition. We also simulated cases (not shown) without any wall radiation as well cases with lower wall temperature (600 K) and found that does not affect any conclusions regarding spray evolution. Diesel spray is injected at 1,000 bar pressure and 320 K temperature near the center of the cylinder. The injection starts at 10 crank-angle degree (CAD) before top dead center (bTDC) and ends at top dead center (TDC). Total mass of Diesel fuel injected is 61 mg over 10 CAD. The nozzle exit diameter is 196 μm and spray cone angle is 10°. The spray injection angle is 14° from the cylinder head. The nozzle discharge coefficient is taken as 0.9 and the droplet size distribution is determined from a Rosin-Rammler distribution. The minimum and maximum diameters for the distribution is 0.8 μm and 80 μm, and the spreading factor is taken as 3 [31]. The secondary breakup of spray is modeled using the Reitz-Diwakar breakup model [47, 48, 49]. Stochastic collision, and surface film effects are neglected. A standard gradient dispersion model is used and spray parcels are assumed to rebound upon hitting walls [31].

Two coupled transient Reynolds' averaged simulations are performed for this hypothetical engine. In each case the standard compressible $k - \varepsilon$ turbulence model with standard wall functions [44, 31] are used, Diesel chemistry is represented by a 34-species skeletal n-heptane mechanism [53], and gas phase spectral properties are evaluated using a LBL database of CO_2, CO, and H_2O obtained from the HITEMP spectroscopic database [43]. Simulations are carried out on a layered moving mesh representing a 45° sector surrounding one injector with 19,250 cells. In one simulation only gas-phase radiation is considered, whereas in the other, along with gas-phase radiation, spray radiation is also considered using the spectral property table and semi-transparent correlation for absorption efficiency formulation. Although detailed chemistry and radiation models are included in these high-fidelity simulations, no interaction between turbulence, chemistry, and radiation has been considered. Study of turbulence, chemistry, and radiation interaction is left for future study. These detailed simulations are performed to test the robustness of the solver, identify possible direct first-order effect of spray radiation in such high-fidelity simulations, and to get a preliminary sense of possible effects of detailed chemistry. Again, it is emphasized here that the goal of this simulation is to look at the effect of spray radiation and not to validate or investigate accuracy of spray or combustion submodels.

The evolution of the liquid spray and global mean quantities from the two simulations are presented in Fig. 9. Figure 9(a) shows the total mass evaporated from the liquid spray and the liquid penetration length during the the injection period. Effects of spray radiation on these two quantities is negligible. This is expected because spray evaporation is dominated by convective heat transfer. Figure 9(b) presents mean pressure and temperature in the domain during the period of simulation. It is worth noting here that from the pressure and temperature trace we can see that the ignition starts close to 3 CAD bTDC. Spray radiation does not affect global mean pressure and temperature trace appreciably.

The relative magnitudes of convective and radiative heat transfer to the spray were also investigated. Similar to the combustion bomb case, the rate of convective heat transfer was found to be orders of magnitude larger than the rate of

radiative heat transfer for spray parcels. Although the hypothetical case presented here does not represent all possible configurations of a Diesel engine, it indicates the relative importance, or lack thereof, of radiative heating compared to convective heating in the evolution of spray droplets in closed, high-pressure systems with high injection velocity. The actual value of the ratio of the two heat transfer rates will vary with engine conditions, such as injection pressure, in-chamber pressure and temperature distribution, presence of emitting participating media, temperature of walls, etc. But nonetheless, it is not expected that the influence of radiative heating will be noticeable in spray evolutions in any scenario.

Although spray radiation does not affect global quantities greatly, it may affect local scalar distributions. To investigate that, we looked at scalar distributions on a radial cutting plane that divides the sector mesh by half. We present results on this cutting plane at two time instances: first at 2.5 CAD bTDC, when ignition has started robustly and spray is still being injected; and at 2 CAD after TDC (aTDC), when all liquid spray has evaporated. Figure 10, which shows the local temperature distributions at 2.5 CAD bTDC, indicates that including spray radiation produces no noticeable differences in temperature. This is true in the post-injection region (2 CAD aTDC) also (not shown). However, small effects due to spray radiation was observed on several minor species (e.g., CH_3, C_3H_4, C_2H_2, etc.), which are usually more sensitive to small temperature fluctuations than major species [54, 23]. The exact sensitivities of these minor species on temperature fluctuations depends on several factors such as the underlying gas-phase chemical mechanism, flow conditions, etc., and are beyond the scope of the current study. However, as a starting point, here we only present effects of spray radiation on the distribution of mass fraction of C_2H_2 because of its importance in soot formation. The difference, albeit small, is more noticeable in the post-injection zone (2 CAD aTDC, Fig. 11). To show the difference more clearly, a radial profile of C_2H_2 mass fraction along the region of peak C_2H_2 concentration (line shown in Fig. 11) is presented in Fig. 12. The magnitude of the peak mass fraction is slightly (10%) higher in the case with spray radiation. The total mass of C_2H_2 is also marginally (7%) higher with spray radiation at this time. C_2H_2 is an important precursor to polycyclic aromatic hydrocarbons (PAHs) and soot. Soot is also highly sensitive to local temperature, and concentrations of C_2H_2 and PAHs. Therefore, small differences in C_2H_2 concentration may have noticeable effects on soot production in the simulation. This trend is similar to a previous study [23], where in a laminar counterflow configuration, researchers observed that inclusion of spray in radiation model slightly increased soot production, but did not affect the temperature distribution. Since, in the current study, our focus is to develop an accurate and efficient spray radiation model, no soot model was included in the coupled simulation. A quantitative analysis of the effects of spray radiation on soot production in engines is left for future study.

5. Conclusion

In this work a multiphase photon Monte Carlo (PMC) method, for both Lagrangian and Eulerian frameworks, was developed for coupled heterogeneous combustion simulations. Emission from the cold spray is neglected, and droplets are assumed to be large and isotropically scattering. Droplet loading is assumed to be small enough to guarantee independent scattering.

Both the Eulerian and Lagrangian multiphase PMC solvers were first validated in simple configurations, for which exact solution are available. The computational cost of the Lagrangian PMC is much higher than the Eulerian PMC primarily due to differences in ray-spray interaction schemes employed in these two models.

In a typical combustion configuration variations in complex index of refraction of the fuel were found to affect the absorption by the spray. Among the three models used for complex index of refraction, the tabulated spectral data yielded the most absorption by the spray, whereas the spectral correlation produced the least. Three optical models were introduced: a normal incidence approximation, Dunkel's relation for nonconductors, and the semi-transparent correlation. It was found that the first two models, *i.e.*, assuming opaque droplets, leads to overestimation of droplet

absorptance. Impact of scattering was found to be negligible in all cases. There were no significant differences in computational cost for different models.

Finally, the solver was used for coupled simulations for high-pressure spray combustion to evaluate the impact of multiphase radiation. It was found that due to the high injection velocity and small droplet size, convective heat transfer to the droplets was orders of magnitude larger than radiative heat transfer. Since in any practical engine the ambient gas temperature is expected to be at least a couple of hundred degrees higher than droplet inlet temperature, and injection velocity is expected to be very high, multiphase radiation is not expected to impact evolution of the liquid spray directly. In a hypothetical engine-relevant condition, spray radiation was found not to impact global parameters such as mean pressure and temperature traces. It was also found that spray radiation does not impact temperature distribution. However, it does have small effects on the distribution of minor species relevant to soot formation.

In this study we presented a detailed analysis of effects of multiphase radiation on spray combustion with most accurate radiative property data currently available for participating media. We chose a hypothetical engine condition with extreme wall temperatures to investigate possible effects of radiation on spray evolution under typical engine-relevant conditions. While the impact of radiative heating on spray evaporation is expected to be insignificant as long as injection pressure and ambient gas temperature are high, the impact of the spray radiation on the overall combustion dynamics may vary depending on local pressure, injection timing and duration, nozzle properties, ignition delay, fuel properties, exhaust gas recirculation (EGR), loading, etc. In the current simulation of hypothetical operating condition, the impact of spray radiation is seen only on minor species and not on major species or temperature. Therefore if a study requires detailed modeling of minor species such as in predicting pollutants like NO_x and soot, accurate modeling of spray radiation may be required particularly in extreme conditions such as high EGR and high load. In spray combustion configurations, where injection pressure is low, ignition delay is large, and significant amount of soot is formed, spray radiation may have non-negligible effects on global parameters via its effects on minor species. A more detailed study on turbulence-chemistry-radiation-soot interaction and effect of spray radiation on soot and NO_x using a detailed soot model for a real engine is left for future. Additionally combustion configurations, where the spray is not used as a fuel, such as flame quenching by water sprays, spray radiation is expected to have some effect on global heat transfer rates. Such a configuration, however, is beyond the scope of the current study.

It is emphasized here that the above observation only pertains to effects of spray radiation, and is not about effects of gas-phase radiation. Gas radiation is expected to impact overall heat loss characteristics from the engine, particularly during the post-ignition expansion stroke [55, 30]. Moreover, gas-phase radiation may alter the local temperature field, thereby altering the convective heat transfer to the spray and affecting spray evolution. Evaluation of the importance of gas radiation in engine-relevant conditions is beyond the scope of the current study and is left for future study.

Lastly, we would like to point out that the current study is focused only on high-pressure combustion of Diesel fuel. The trends seen here cannot be generalized to other heterogeneous combustion configurations. Impact of multiphase radiation is expected to be much stronger in coal combustion, where the hot coal particles are expected to lose significant amounts of energy by radiative cooling [56, 57]. The PMC solver presented here has already been extended for such applications [57, 58]. Additionally, the multiphase PMC solver can be used in coupled simulations of combustion in the presence of a nonemitting liquid spray (instead of liquid fuel), such as simulations of fire extinction through water sprays.

Acknowledgment

This work has been supported by the NSF/DOE Collaborative Research Award No. 1258635 and by the AFOSR Contract No. FA8650-15-C-2543. Authors would also like to thank Mr. Chandan Paul and Dr. D. C. Haworth for their help with spray and chemistry models.

[1] J. Randrianalisoa, D. Baillis, Radiative properties of densely packed spheres in semitransparent media: A new geometric optics approach, J. Quant. Spectrosc. Radiat. Transfer 111 (10) (2010) 1372–1388.

[2] J. Randrianalisoa, D. Baillis, Radiative transfer in dispersed media: Comparison between homogeneous phase and multiphase approaches, J. Heat Transfer 132 (2) (2010) 023405.

[3] J. F. Sacadura, D. Baillis, Experimental characterization of thermal radiation properties of dispersed media, Int. J. Therm. Sci. 41 (2002) 699–707.

[4] L. A. Dombrovsky, D. Baillis, Thermal Radiation in Disperse Systems: An Engineering Approach, Begell House, New York, 2010.

[5] S. Sazhin, Droplets and sprays, Springer-Verlag, London, 2014.

[6] W. P. Jones, S. Lyra, S. Navarro-Martinez, Numerical investigation of swirling kerosene spray flames using Large Eddy Simulation, Combust. Flame 159 (2012) 1539 – 1561.

[7] G. A. E. Godsave, Studies of the combustion of drops in a fuel spray – the burning of single drops of fuel, Proc. Combust. Symp 4 (1953) 818–830.

[8] S. S. Sazhin, T. Kristyadi, W. A. Abdelghaffar, M. R. Heikal, Models for fuel droplet heating and evaporation: Comparative analysis, Fuel 85 (2006) 1613 – 1630.

[9] J. R. Yang, S. C. Wong, On the discrepancies between theoretical and experimental results for microgravity droplet evaporation, Int J. Heat and Mass Trans 44 (2001) 4433–4443.

[10] T. Kitano, J. Nishio, R. Kurose, S. Komori, Effect of ambient pressure, gas temperature and combustion reaction on droplet evaporation, Combust. Flame 161 (2014) 551–564.

[11] C. C. Tseng, R. Viskanta, Effect of radiation absorption on fuel droplet evaporation, Combust. Sci. Techol. 177 (2005) 1511–1542.

[12] N. Mascarenhas, I. Mudawar, Analytical and computational methodology for modeling spray quenching of solid alloy cylinders, Int. J. Heat Mass. Trans. 53 (2010) 5871–5883.

[13] S. Hostikka, K. McGrattan, Numerical modeling of radiative heat transfer in water sprays, Fire Safety Journal 41 (2006) 76–86.

[14] S. Maruyama, H. Nakai, A. Sakurai, A. Komia, Evaluation method for radiative heat transfer in polydisperse water droplets, J. Quant. Spectrosc. Radiat. Transfer 109 (2008) 1–15.

[15] E. P. Keramida, A. N. Karayannis, A. G. Boudouvis, N. C. Markatos, Numerical modeling of radiant heat attenuation through water mist, Comb. Sci. Technol. 159 (2000) 351–371.

[16] J. Dembele, S. Wen, Analysis of the screening of hydrogen flares and flames thermal radiation with water sprays, Int. J. of Hydrogen Energy 39 (2014) 6146 – 6159.

[17] C. Wang, Y.-C. Du, J.-G. Zhang, C.-H. Wang, Fast calculating method for radiative heat shielding by polydisperse and anisotropic scattering water sprays, Optik 127 (2016) 43–47.

[18] S. Lechêne, Z. Acem, G. Parent, A. Collin, P. Boulet, Radiative shielding by water mist: comparison between downward, upward and impacting injection of droplets, J. of Physics 369 (2012) 012027–1–012027–10.

[19] S. Lechêne, Z. Acem, G. Parent, G. Jeander, P. Boulet, Upward vs downward injection of droplets for the optimization of a rdaitive shield, Int. J. of Heat and Mass Transfer 54 (2011) 1689–1697.

[20] S. Dembele, A. Delmas, J. F. Sacadura, A method of modeling the mitigation of hazardous fire thermal radiation by water spray curtains, J. of Heat Transfer 119 (1997) 746–753.

[21] Y. W. Yan, J. X. Zhao, J. Z. Zhang, Y. Liu, Large-eddy simulation of two-phase spray combustion for gas turbine combustors, Applied Thermal Engineering 28 (2008) 1365–1374.

[22] Z. Chen, J. Wen, B. Xu, S. Dembele, Large eddy simulation of a medium-scale methanol pool fire using the extended eddy dissipation concept, Int. J. of Heat and Mass Trans. 70 (2014) 389–408.

[23] H. Watanabe, R. Kurose, S. Komori, H. Pitsch, Effects of radiation on spray flame characteristics and soot formation, Combust. Flame 152 (2008) 2–13.

[24] A. Fujita, H. Watanabe, R. Kurose, S. Komori, Two-dimensional direct numerical simulation of spray flames - part 1: Effects of equivalence ratio, fuel droplet size and radiation, and validity of flamelet model, Fuel 104 (2013) 515–525.

[25] H. El-Asrag, A. Iannettib, S. V. Apte, Large eddy simulations for radiation-spray coupling for a lean direct injector combustor, Combust. Flame 161 (2014) 510–524.

[26] M. P. Menğuc, R. Viskanata, C. R. Ferguson, Multidimensional modeling of radiative heat transfer in diesel engines, SAE Tech. Pap. 850503.

[27] G. Borman, K. Nishiwaki, Internal combustion engine heat transfer, Prog. Energy Combust. Sci. 13 (1987) 1–46.

[28] J. Abraham, V. Magi, Application of the discrete ordinates method to compute radiant heat loss in a diesel engine, Numer. Heat Transf. A 31 (1997) 597–610.

[29] J. Wiedenhoefer, R. Reitz, A multidimensional radiation model for diesel engine simulations with comparison to experiment, Numer. Heat Transf. A 44 (2003) 665–682.

[30] V. Raj Mohan, Development and application of a transported probability density function model for advanced compression-ignition engines, Ph.D. thesis, The Pennsylvania State University (2014).

[31] OpenCFD, Openfoam 2.2.x, www.openfoam.org (2013).
URL `www.openfoam.org`

[32] M. F. Modest, Radiative Heat Transfer, 3rd Edition, Academic Press, New York, 2013.

[33] A. Tuntomo, Transport phenomena in a small particle with internal radiant absorption, Ph.D. thesis, University of California at Berkeley, Berkeley, CA (1990).

[34] L. A. Dombrovsky, S. S. Sazhin, S. V. Mikhalovsky, R. Wood, M. R. Heikal, Spectral properties of diesel fuel droplets, Fuel 82 (2003) 15–22.

[35] L. A. Dombrovsky, Thermal radiation from nonisothermal spherical particles of a semitransparent material, Intl. J. Heat Mass Transfer 43 (9) (2000) 1661–1672.

[36] R. V. Dunkel, Emissivity and inter-reflection relationships for infinite parallel specular surfaces, in: S. Katzoff (Ed.), Symposium on thermal radiation of solids NASA SP55, 1965, pp. 39 – 44.

[37] L. A. Dombrovsky, Spectral model of absorption and scattering of thermal radiation by diesel fuel droplets, High Temp. 40 (2002) 242–248.

[38] A. Wang, M. F. Modest, Photon Monte Carlo simulation for radiative transfer in gaseous media represented by discrete particle fields, J. Heat Transfer 128 (2006) 1041–1049.

[39] T. Ren, M. F. Modest, Hybrid wavenumber selection scheme for line-by-line photon Monte Carlo simulations in high-temperature gases, J. Heat Transfer 135 (8) (2013) 084501.

[40] D. C. Haworth, Progress in probability density function methods for turbulent reacting flows, Progr. Energy Combust. Sci. 16 (2010) 168–259.

[41] J. Cai, X. Zhao, M. Modest, D. Haworth, Nongray radiation modelings in Eulerian–Lagrangian methods for pulverized coal flames, in: Proceedings of the First Thermal and Fluids Engineering Summer Conference, 2015.

[42] R. Marquez, M. F. Modest, Spectral photon monte-carlo with energy splitting across phases for gas-particle mixtures, 22nd National and 11th International ISHMT–ASME Heat and Mass Transfer Conference 2013, Kharagpur, India, 2013.

[43] L. S. Rothman, I. E. Gordon, R. J. Barber, H. Dothe, R. R. Gamache, A. Goldman, V. I. Perevalov, S. A. Tashkun, J. Tennyson, HITEMP, the high-temperature molecular spectroscopic database, J. Quant. Spectrosc. Radiat. Transfer 111 (15) (2010) 2139–2150.

[44] S. El-Tahry, k-ε equation for compressible reciprocating engine flows, J. Energy 7 (1983) 345–353.

[45] J. Broukal, J. Hájek, J. Jedelský, Effervescent atomization of extra-light fuel-oil : Experiment and statistical evaluation of spray characteristics, in: ILASS – Europe 2010, 23rd Annual Conference on Liquid Atomization and Spray Systems, no. September, Brno, Czech Republic, 2010, pp. 1–10.

[46] S. D. Sovani, P. E. Sojka, A. H. Lefebvre, Effervescent atomization, Prog. Energy Combust. Sci. 27 (4) (2001) 483–521.

[47] R. Reitz, Modelling atomization processes in highpressure vaporizing sprays, Atomization and Spray Technology 3 (1987) 309–337.

[48] R. Reitz, R. Diwakar, Effect of drop breakup on fuel sprays, SAE Tech. paper series 860469.

[49] R. Reitz, R. Diwakar, Structure of high-pressure fuel sprays, SAE Tech. paper series 870598.

[50] W. Ranz, W. Marshal, Evaporation from drops: Parts 1 and 2, Chemical Engineering Progress 48 (1952) 141–147,173–180.

[51] B. Kegl, M. Kegl, S. Pehan, Green Diesel Engines: Biodiesel Usage in Diesel Engines, Springer-Verlag, London, 2013.

[52] S. Singh, R. D. Reitz, M. P. B. Musculus, T. Lachaux, Validation of engine combustion models against detailed in-cylinder optical diagnostics data for a heavy-duty compression-ignition engine, Int. J. Engine Res. 8 (2007) 97–126.

[53] A. Patel, S. C. Kong, R. D. Reitz, Development and validation of a reduced reaction mechanism for HCCI engine simulations, SAE Tech. Pap. 2004-01-0558.

[54] G. Pal, A. Gupta, M. F. Modest, D. C. Haworth, Comparison of accuracy and computational expense of radiation models in simulation of nonpremixed turbulent jet flames, Combust. Flame 162 (2015) 2487–2495. doi:10.1016/j.combustflame.2015.02.017.

[55] M. F. Modest, D. C. Haworth, Radiative heat transfer in turbulent combustion systems, Springer, 2015.

[56] J. Cai, M. Handa, M. F. Modest, Eulerian–Eulerian multi-fluid methods for pulverized coal flames with nongray radiation, Combust. Flame 162 (2015) 1550–1565.

[57] B. Wu, S. Roy, M. F. Modest, X. Zhao, Monte Carlo modeling of radiative transfer in a pulverized coal jet flame, in: Proceedings of the 8th International Symposium on Radiative transfer, RAD-16, Capadocia, Turkey, 2016.

[58] B. Wu, S. P. Roy, X. Zhao, M. F. Modest, Effect of multiphase radiation on coal combustion in a pulverized coal jet flame, J. Quant. Spectros. Radiat. Transfer In press. doi:10.1016/j.jqsrt.2017.03.017.

Appendix A: Line-by-line data for unboiled Diesel

The spectral variation of complex index of refraction of unboiled Diesel fuel for automobiles is taken from [34]. A reconstruction of this data is shown Fig. 13. Note that the complex index of refraction data is only available for $2 < \lambda < 10\,\mu$m.

Appendix B: Correlation for complex index of refraction for Diesel

The correlation used for Diesel fuel (Eqn. 5) is taken from [4]. The constants used in the correlation for unboiled Diesel fuel for automobiles are as follows

$$n_0 = 1.46 \tag{33a}$$

$$\lambda_m = 3.4 \tag{33b}$$

$$\gamma = \begin{cases} -b_1 & 2.0\,\mu\text{m} < \lambda < 2.2\,\mu\text{m} \\ 10(b_1 - 2.3)(\lambda - 2.2) - b_1 & 2.2\,\mu\text{m} < \lambda < 2.3\,\mu\text{m} \\ 4(b_2 - 2.3)(\lambda - 2.8)^2 - b_2 & 2.3\,\mu\text{m} < \lambda < 3.3\,\mu\text{m} \\ 21(\lambda - 3.3) - 2.3 & 3.3\,\mu\text{m} < \lambda < 3.4\,\mu\text{m} \\ 12.5(\lambda - 3.8)^2 - 2,2 & 3.4\,\mu\text{m} < \lambda < 3.8\,\mu\text{m} \\ (b_3 - 2.2)\left(\frac{\lambda - 4.9}{1.1}\right)^2 - b_3 & 3.8\,\mu\text{m} < \lambda < 6.0\,\mu\text{m}, \end{cases} \tag{33c}$$

$$b_1 = 4.0 \tag{33d}$$

$$b_2 = 3.4 \tag{33e}$$

$$b_3 = 3.8 \tag{33f}$$

where the wavelength, λ, is measured in μm.

Table 1: Summary of submodels and assumptions used in coupled simulations.

Submodels	Combustion Bomb	Engine-relevant configuration
Spray	Rosin-Rammler distribution [31]	
	Reitz-Diwakar secondary breakup model [47, 48, 49]	
	No dispersion	Gradient dispersion model [31]
	No stochastic collision	
	No film effects	
	Perfect rebound at wall	
Flow	Unsteady RAS with standard compressible $k-\varepsilon$ model [44, 31]	
Chemistry	Global chemistry with five species [31]	Detailed chemistry with 34 species [53]
Convection	Ranz-Marshall correlation [50]	
Radiation	Spray radiation models as discussed in respective sections	
	LBL treatment of gas radiation using HITEMP data [43]	
	Emitting black wall at the same temperature of adjacent gas	Emitting black walls at specified temperatures

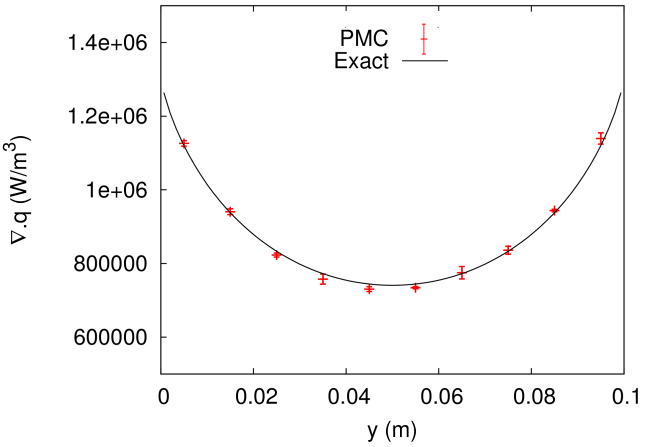

Figure 1: Comparison of divergence of radiative heat flux for a one-dimensional slab filled only with a homogeneous spray and bounded by hot black walls. Error bars represent one standard deviation.

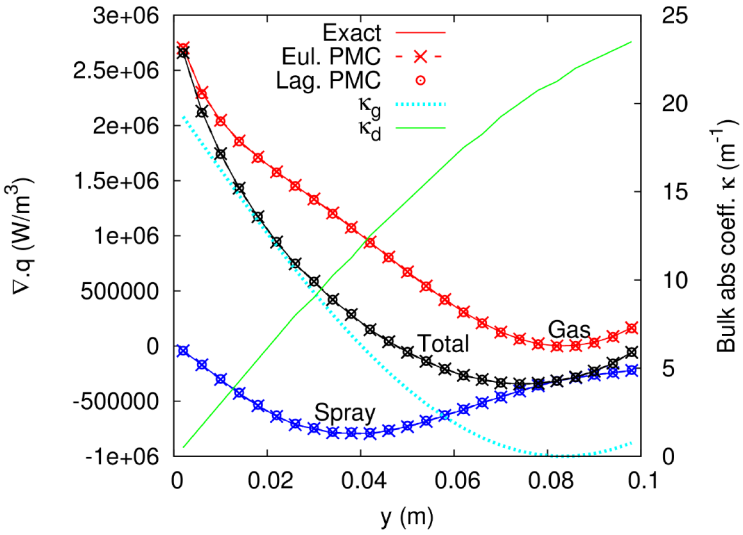

Figure 2: Comparison of divergence of radiative heat flux from the Eulerian and Lagrangian PMC for a one-dimensional slab with cold black walls and mixtures of gas and spray. The bulk absorption coefficients for both phases are plotted on the secondary y axis. Individual contribution of each phase is also noted.

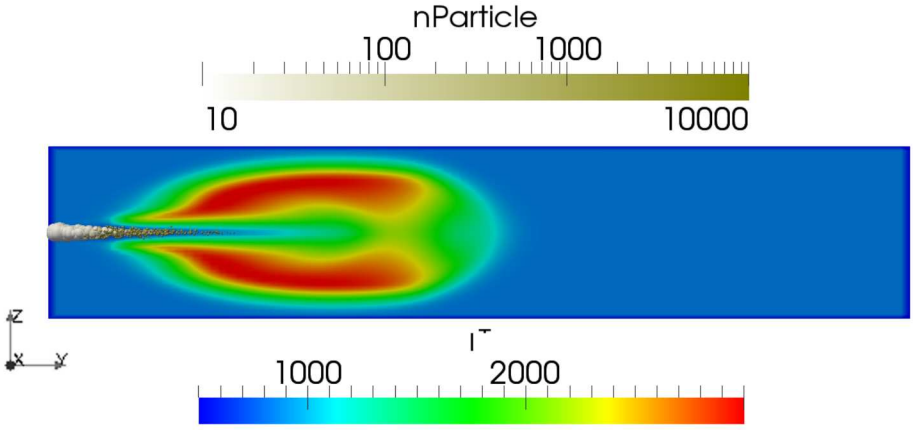

Figure 3: Snapshot of a high-pressure constant-volume combustion bomb used for parametric study of spray radiation models. The size of a parcel is scaled by the diameter of the droplets in it. The quantity `nParticle` refer to number of droplets in each parcel. Note logarithmic scale for `nParticle`.

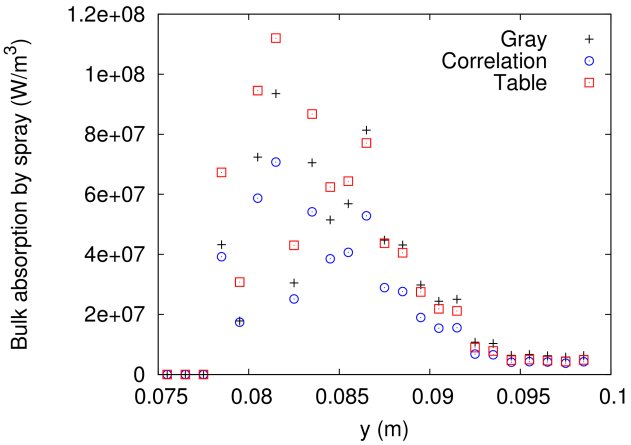

Figure 4: Comparison of absorption by spray in combustion bomb snapshot due to different spectral models using the semi-transparent correlation.

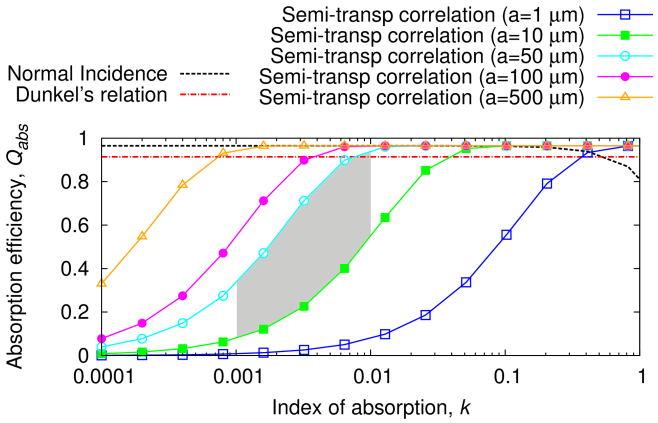

Figure 5: Comparison of absorption efficiencies calculated from different optical models for an incident ray of 3 μm for different droplet radii (a).

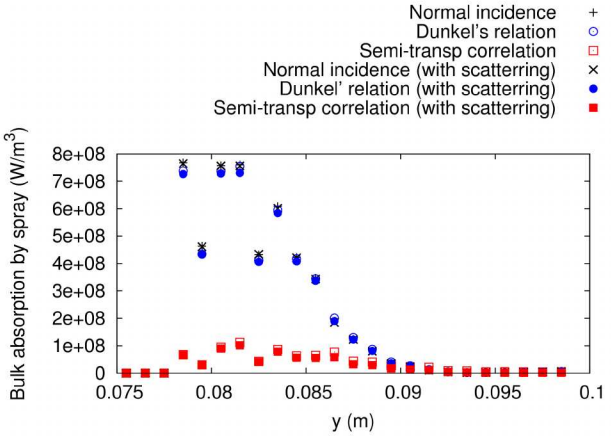

(a) Absorption by spray from different optical models

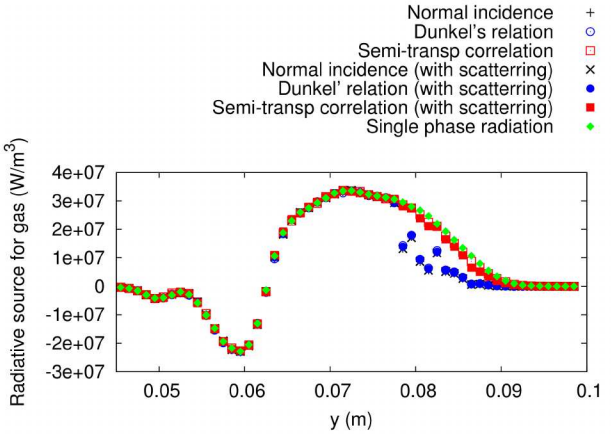

(b) Radiative source term for gas from different optical models

Figure 6: Comparison of radiative source terms in the combustion bomb snapshot for spray and gas phases due to different optical models and scattering.

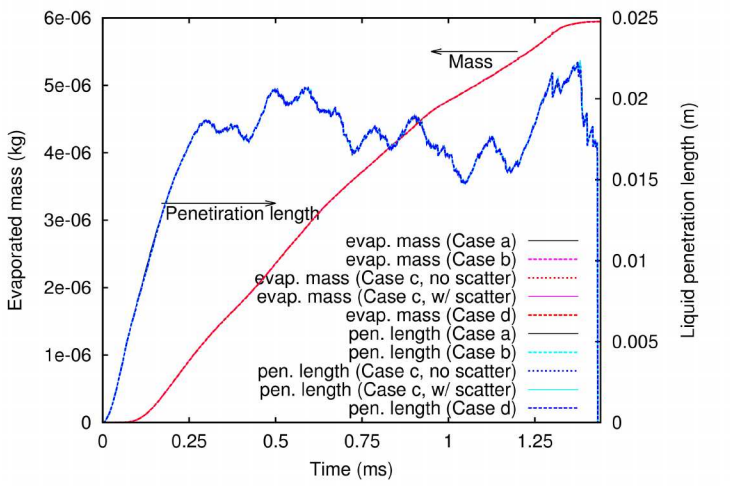

Figure 7: Spray evolution profile for the high-pressure constant volume combustion bomb. Red and magenta lines show cumulative evaporated liquid mass in the spray jet in the domain, and blue and cyan lines represent liquid penetration length.

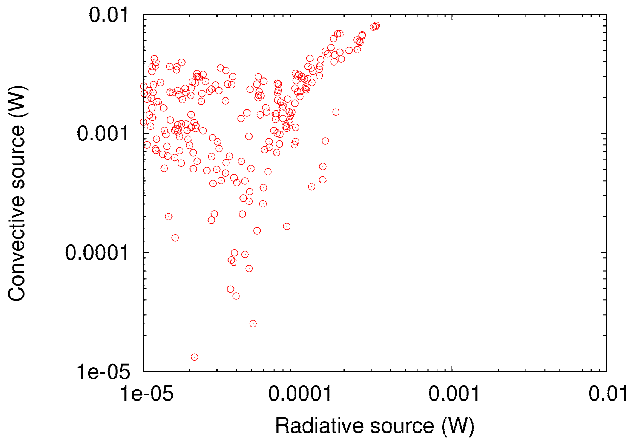

Figure 8: Relative magnitude of convective and radiative heat transfer rates for droplets for a hypothetical snapshot. Each point represents a parcel.

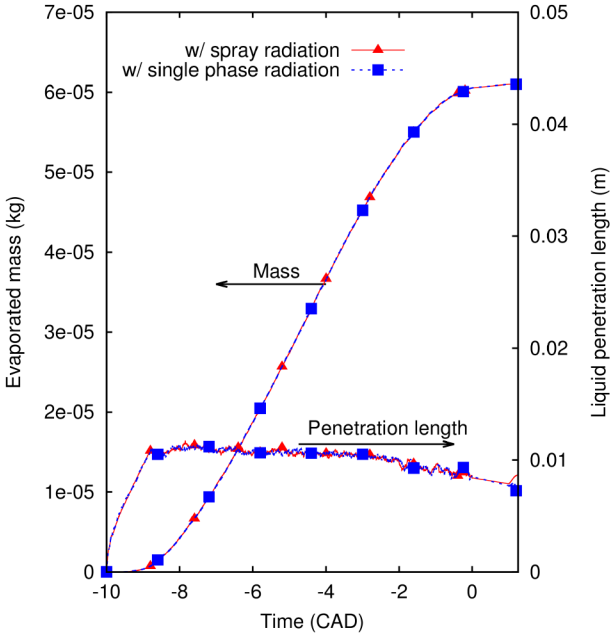

(a) Global liquid quantities

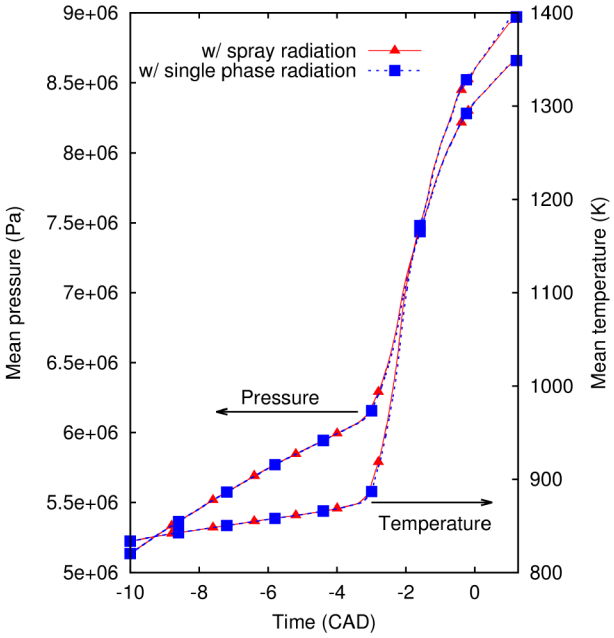

(b) Mean pressure and temperature

Figure 9: Spray evolution profile from the hypothetical engine simulation with and without spray radiation.

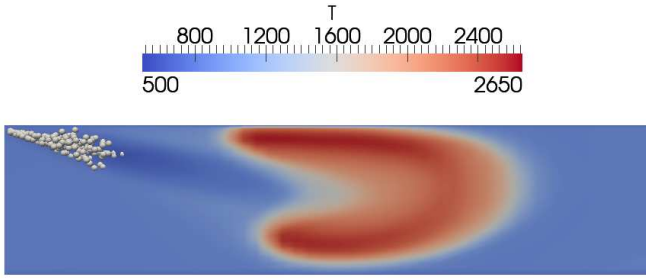

(a) With single-phase radiation

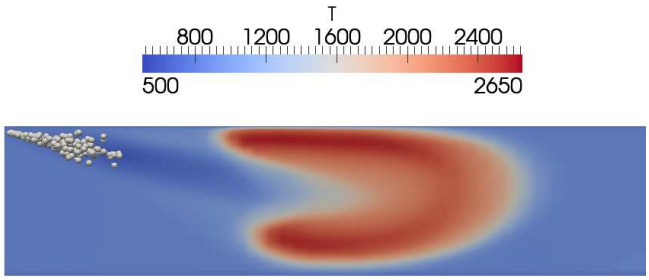

(b) With spray radiation using the semi-transparent correlation

Figure 10: Differences in temperature distribution due to spray radiation in the hypothetical engine after start of ignition (at 2.5 CAD bTDC).

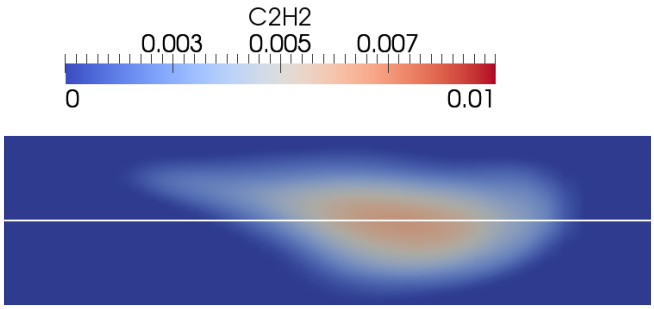

(a) With single-phase radiation

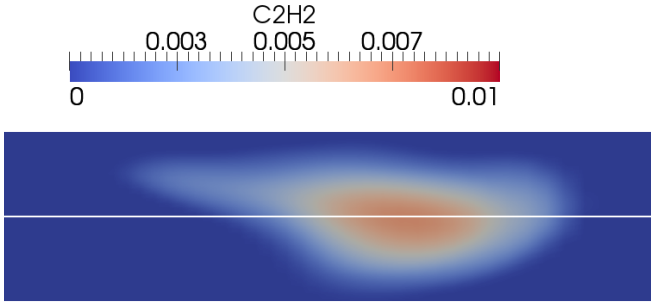

(b) With spray radiation using the semi-transparent correlation

Figure 11: Differences in C_2H_2 mass fraction distribution due to spray radiation in the hypothetical engine at 2 CAD after the end of injection (at 2 CAD aTDC).

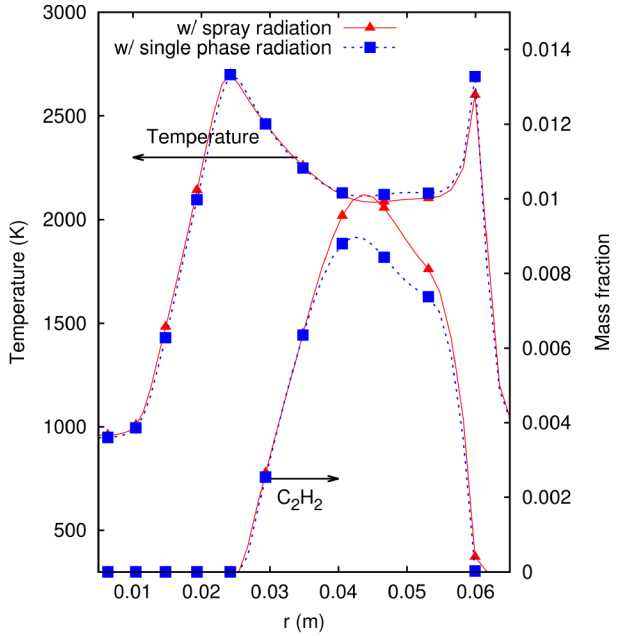

Figure 12: Temperature and acetylene mass fraction along a radial line of the domain at 2 CAD aTDC.

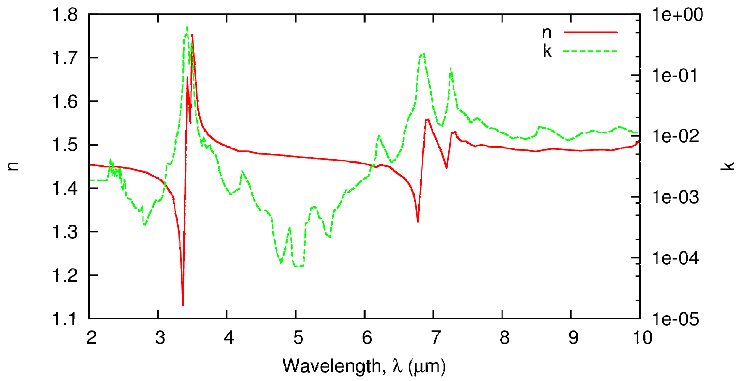

Figure 13: Spectral variation of complex index of refraction for unboiled Diesel fuel for automobiles, reconstructed from the data presented in [34].